Han-xue Cao*, Xue-yan Wu, Hui-min Liao and Meng-yao Hao

Development of Processing Maps for AZ81E Magnesium Alloy

DOI 10.1515/htmp-2016-0082
Received April 19, 2016; accepted December 30, 2016

Abstract: The hot deformation characteristics of a AZ81E magnesium alloy are studied in the RANGE temperatures from 340 to 430 °C and strain rates ranging between 0.003 and 3.0 s^{-1} utilizing hot compression tests. Combining Arrhenius equation and Zener-Hollomon parameter, the high temperature flow stress model is proposed and the average activation energy is 166.15 kJ/mol. Processing maps for hot working are developed on the basis of the efficiency of power dissipation with changing temperatures and strain rates. The power dissipation map reveals that the optimum hot working domain is the temperature range of 390–400 °C and strain rate range of 0.03–0.3 s^{-1}.

Keywords: AZ81E, flow stress, hot compression tests, processing maps, hot working parameters

Introduction

The structural applications of magnesium alloys in aerospace and automobile industries are rising gradually in view of their low density, high damping capacity and high specific strength [1, 2]. Casting technique is widely used in magnesium alloys. But castings are restricted in structural applications because of their low properties. Moreover, magnesium with the hexagonal close-packed (hcp) structure can only initiate a limited number of slip systems, which basal slip preferentially takes place because the critical resolved shear stress (CRSS) for the basal slip is lower than that for prismatic and pyramidal slips at room temperature. Liao Hui-min suggested that the addition of Ce to AZ81 magnesium alloy is reported to be very effective for developing its strength, elongation and hardness [3]. But the research on the hot deformation behavior of AZ81E magnesium alloy has been scarcely reported in references.

The present investigation aims to construct the high temperature flow stress model of AZ81E and develop processing map for hot working of AZ81E including optimizing its hot workability. The workability of AZ81E is specified by its flow stress, which depends on the forming temperatures and deformation rates. Processing maps are developed on the basis of the dynamic material model, which is recently reviewed by Prasad and Sheshacharulu [4, 5]. The model considers the work piece as a dissipater of power and the whole power dissipated (P) is composed of two complementary parts: the G content and the J co-content. G content represents the temperature rise dissipation and J co-content represents microstructural dissipation. The factor that partitions the power between J and G is the strain rate sensitivity (m) of the flow stress (σ), and the J co-content being given by:

$$J = \sigma\dot{\varepsilon}m/(m+1) \tag{1}$$

where σ is the flow stress, $\dot{\varepsilon}$ is the strain rate. Furthermore m is given by:

$$m = \left(\frac{\partial J}{\partial G}\right)_{T,\varepsilon} = \left(\frac{\partial \ln \sigma}{\partial \ln \dot{\varepsilon}}\right)_{T,\varepsilon} \tag{2}$$

In an ideal linear dissipater condition, $m = 1$ and $J = J_{max} = \sigma\dot{\varepsilon}/2$. In a non-linear dissipater condition, the efficiency of power dissipation may be expressed in terms of a dimensionless parameter:

$$\eta = J/J_{max} = 2m/(m+1) \tag{3}$$

The variation of the efficiency with temperature and strain rate constitutes a processing map, which exhibits different domains that should be correlated with specific microstructural processes. According to criterion developed by Prasad [6], flow instability will occur if:

$$\xi(\dot{\varepsilon}) = \partial \ln[m/(m+1)]/\partial \ln \dot{\varepsilon} + m\langle 0 \tag{4}$$

The variation of $\xi(\dot{\varepsilon})$ with temperature and strain rate constitutes the instability map which may be

***Corresponding author: Han-xue Cao,** College of Materials Science and Engineering, Chongqing University, Chongqing 400030, China; National Engineering Research Center for Magnesium Alloys, Chongqing University, Chongqing 400030, China, E-mail: hanxue_cao@cqu.edu.cn
Xue-yan Wu, College of Materials Science and Engineering, Chongqing University, Chongqing 400030, China
Hui-min Liao, School of Materials Science and Engineering, Xihua University, Chengdu 610039, China
Meng-yao Hao, College of Materials Science and Engineering, Chongqing University, Chongqing 400030, China

superimposed on the processing map to delineate instability regimes of negative $\xi(\dot{\varepsilon})$values.

With the help of a processing map, it is possible to find out the optimum parameters for designing a metal-working process without resorting to expensive and time-consuming trials and error methods [7–9].

Experimental procedure

The chemical composition (wt. %) of the AZ81E used in present study was as follows: Al, 8.0; Zn, 0.79; MM, 1.2, and balance Mg. The MM was mixed rare-earth enriched with Cerium. The starting material was a squeeze-cast ingot with homogenization treatment at 400 °C for 8 h. Cylindrical specimens of 8 mm diameter and 10 mm height were machined for hot compression testing. The hot compression tests were conducted on Gleeble-1500D thermal simulator testing machine. The specimens were compressed at the temperature and the strain rate ranges 340–430 °C and 0.003–3.0 s^{-1}, respectively. The specimens were heated in a rate of 10 °C/s and kept for 3 min before the hot compression test. Graphite powder mixed with grease was used as the lubricant in all the experiments. The specimens were deformed up to a true strain of 0.8 and the compression direction was parallel with axis of specimens. Deformed specimens were quenched in water and the cut surface was prepared for microstructure of the cross-section was investigated by the optical microscopy(OM). The load–stroke data obtained in compression were processed to obtain true stress–true elastic strain curves using the standard method. As a function of temperature, strain rate and strain, the flow stress data were obtained from the above curves and used for constructing the power dissipation maps.

Results and discussion

Flow stress

The flow curves of AZ81E at various temperatures from 340 to 430 °C under 0.03 s^{-1} and at various strain rates from 0.003 to 3.0 s^{-1} under 400 °C are shown in Figure 1. It is observed that the flow stress is directly related to both the strain rates and the temperature. Under the constant strain rate, the flow stress gradually deceases as the temperature rises. Moreover, at higher temperatures the stress reaches a maximal value quickly and attains the steady state. With the decrease of temperature, the peak stress corresponds to the higher strain. At the constant temperature, the flow stress increases with the increase of strain rate. At the same time, with the increase of strain rate, the strain goes up obviously at steady state. In addition, the flow stress reaches a peak value rapidly under lower strain rate.

The peak stress and the steady-state stress increase with strain rate and decrease with the temperatures. This is in consequence of the low strain rate providing long time for the nucleation and growth of dynamically recrystallized grains. On the other hand, the higher temperature provides the higher softening rate to balance the increase of strain hardening rate. Furthermore, the dynamic recovery and dynamic recrystallization (DRX) take place under

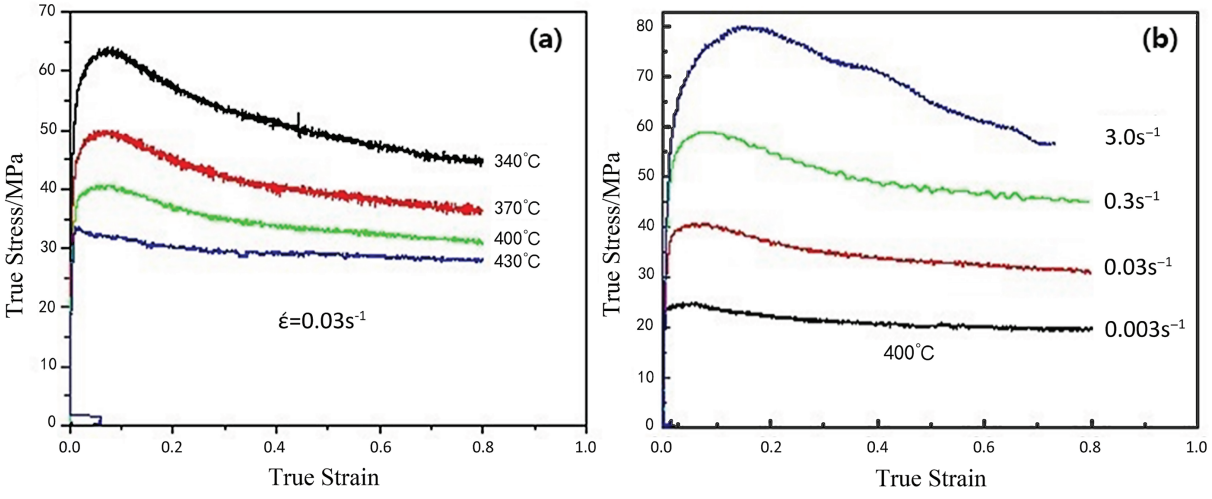

Figure 1: Flow stress and strain curves of AZ81E Mg-alloy.

hot deformation. Owing to the DRX, the flow stress yields a significant reduction [10–12].

The constitutive model for AZ81E

As demonstrated by the curves of AZ81E, the flow stress in hot deformation is related to the strain rate and the temperature. According to the research of hot deformation data, Sellar and Tegart developed an Arrhenius kinetic rate equation which includes the activation energy and the temperature [13]. In addition, at lower stress and higher stress level, the relationship between peak stress and strain rate is described by exponential function and power exponent function, respectively. And the steady-state flow stress is described by hyperbolic function. The equations are as follows:

$$\dot{\varepsilon} = A_1 \sigma^{n_1} \exp\left[\frac{-Q}{RT}\right] \tag{5}$$

$$\dot{\varepsilon} = A_2 \exp(\beta\sigma_p) \exp\left[\frac{-Q}{RT}\right] \tag{6}$$

$$\dot{\varepsilon} = A_3 (\sinh(\alpha\sigma_p))^n \exp\left[\frac{-Q}{RT}\right] \tag{7}$$

where $\dot{\varepsilon}$ is the strain rate; A_1, A_2, A_3 and α, β are constants, n and n_1 are stress exponents, Q is the activation energy, R is the gas constant, T is the temperature, σ is the steady flow stress, σ_p is the peak stress. The logarithm of eqs (5)–(7) are as follows:

$$\ln\dot{\varepsilon} = n_1 \ln\sigma + \ln A_1 - \frac{Q}{RT} \tag{8}$$

$$\ln\dot{\varepsilon} = \beta\sigma_p + \ln A_2 - \frac{Q}{RT} \tag{9}$$

$$\ln\dot{\varepsilon} = n\ln[\sinh(\alpha\sigma)] + \ln A - \frac{Q}{RT} \tag{10}$$

The temperature compensated strain rate parameter (Zener-Hollomon parameter) can be described as:

$$A[\sinh(\alpha\sigma)]^n = \dot{\varepsilon}\exp[Q/RT] = Z \tag{11}$$

So the constitutive equation for analysis of hot deformation is:

$$\sigma = (1/\alpha)\ln\left\{(Z/A)^{1/n} + [(Z/A)^{2/n} + 1]^{1/2}\right\} \tag{12}$$

Through the analysis of eqs (5) and (6), the relationship between peak stress and strain rate of AZ81E at various temperatures is shown in Figure 2. Then, the results of data are as follows: $n_1 = 6.119$, $\beta = 0.111$, $\alpha = 0.0182\ \text{MPa}^{-1}$.

According to the true stress–true plastic strain curves, the relationship between $\ln[\sinh(\alpha\sigma_p)]$ and $\ln\dot{\varepsilon}$ at different temperatures is shown in Figure 3. Moreover, the relationship between $\ln[\sinh(\alpha\sigma_p)]$ and $-1/T$ at different strain rates is seen in Figure 4. The partial derivative equation of eq. (10) is:

$$Q = R\left[\frac{\partial\ln\dot{\varepsilon}}{\partial\ln[\sinh(\alpha\sigma)]}\right]_T \left[\frac{\partial\ln[\sinh(\alpha\sigma)]}{\partial 1/T}\right]_{\dot{\varepsilon}} \tag{13}$$

For the present experiments, α is $0.0182\ \text{MPa}^{-1}$, the activation energy Q is evaluated by using eq. (13) at various temperatures and strain rates. The average value of AZ81E is 166.15 KJ/mol. The activation energy Q usually equals to activation enthalpy ΔH. Influenced by

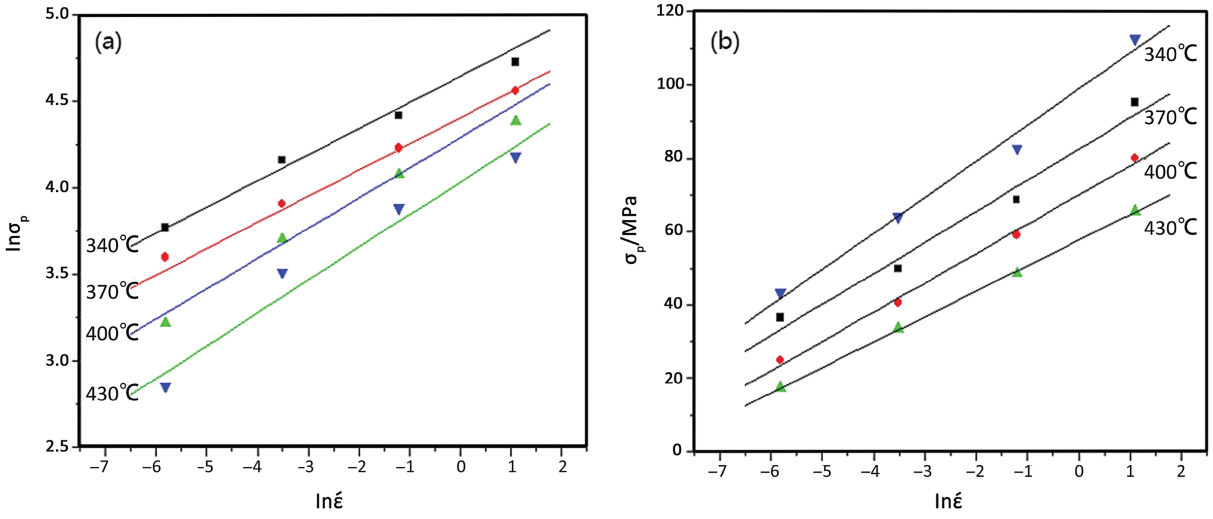

Figure 2: Relationship between peak stress and strain rate according: (a) $\ln\dot{\varepsilon} - \ln\sigma$; (b) $\ln\dot{\varepsilon} - \sigma$.

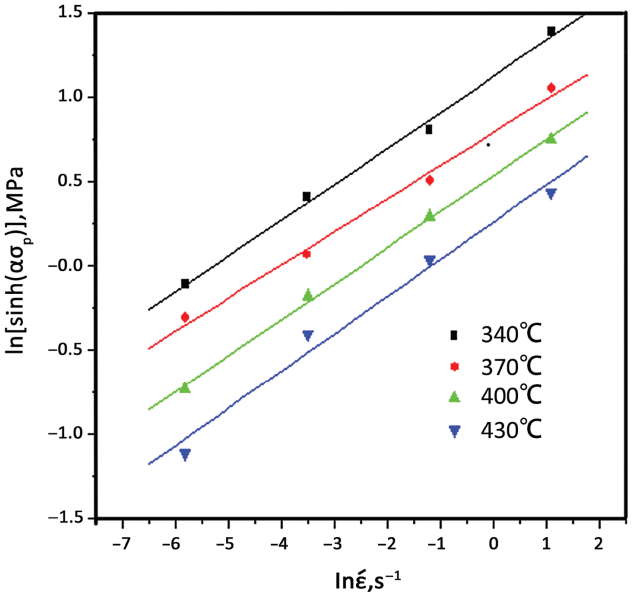

Figure 3: Curves of $\ln[\sinh(\alpha\sigma_p)]$-$\ln\dot{\varepsilon}$ at various temperatures.

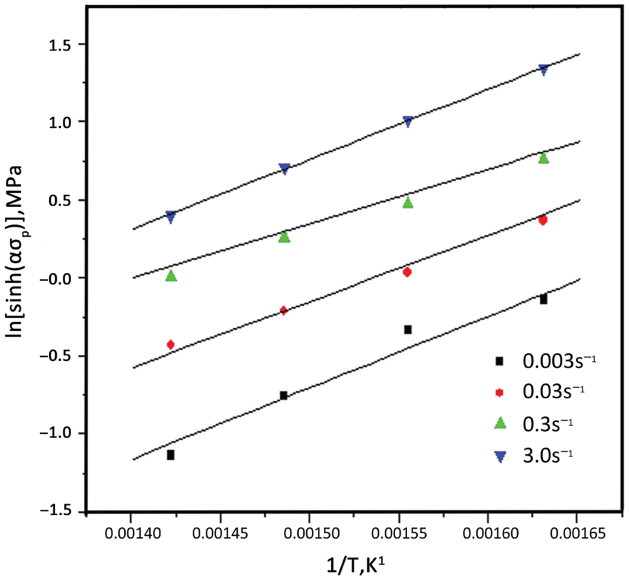

Figure 4: Curves of $\ln[\sinh(\alpha\sigma_p)]$-1/T at various strain rates.

deformation temperature, strain rate and other factors, large numbers of secondary phase particles are precipitated out from AZ81E precursor phase. During the plastic deformation of the alloy, the dispersive distributive particles hinder the dislocation sliding as obstacles, leading the rising of the energy. The activation energy is raised accordingly. However, the dispersive distributive particles of rare-earth phase not only aggravate the dislocation motion but also refine the grain. Such behaviors reduce the energy of the sliding and climbing of dislocations, while the activation energy is reduced at the same time.

Equation (11) indicates a linear relationship exists between log Z and the flow stress. Variation of flow stress with Z parameter for the AZ81E is plotted in Figure 5. The equation can be expressed as follows:

$$\ln Z = 27.42 + 4.35\ln[\sinh(\alpha\sigma_p)] \tag{14}$$

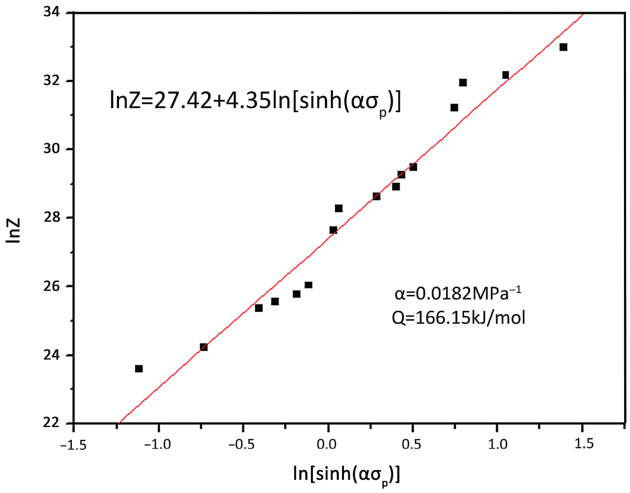

Figure 5: Relationship between Z parameter and flow stress of AZ81E alloy.

And the flow stress equation of AZ81E magnesium alloy is:

$$\sigma = 54.95\ln\left\{(Z/8.098\times10^{11})^{1/4.35} + [(Z/8.098\times10^{11})^{2/4.35}+1]^{1/2}\right\} \tag{15}$$

Where the Z is:

$$Z = \dot{\varepsilon}\exp(166.15\times10^3)/RT \tag{16}$$

Processing maps for AZ81E

As continuum maps, the power dissipation maps are interpreted in terms of the microstructural processes. These maps reveal the limiting temperature and strain rate conditions for the occurrence of fracture and instabilities during the deformation of materials. Typically, at lower temperatures and higher strain rates, void formation at hard particles occurs, while at higher temperatures and lower strain rates, wedge cracking occurs at grain boundary triple junctions. At very high strain rates, instability due to adiabatic shear band formation is the likelihood. The regime marked by the limiting conditions for these processes is defined as “safe” for processing, and in this regime the processes of dynamic recovery

(lower temperatures and strain rates) and DRX (higher temperatures and strain rates) occur. Although Raj considered dynamic recrystallization to be an undesirable feature during flow localization, Gandhi concluded that both dynamic recovery and DRX are desirable processes during hot working of a uniform billet, to keep the flow stresses and rates of work hardening considerably low. In fact, it is observed that DRX can effectively expand the safe working zone by raising the upper bound for cavity nucleation at hard particle boundaries and moving lower bound for wedge crack initiation at grain boundary triple junction [14–16].

The processing maps obtained for AZ81E at a strain of 0.4 and 0.6 are displayed in Figure 6 (a and b), respectively. The contours represent constant efficiency of power dissipation marked as percent and the shaded areas indicate the regions of flow instability.

At 0.4 strain, the domain occurs in the region of 340–430 °C for a strain rate range from 0.003 to 0.1 s^{-1}, with a peak efficiency of around 50 %. The DRX occurs at about 400 °C and 0.003 s^{-1}, with a efficiency of about 43 %. At this temperature, if the strain rate is sufficiently high, the deformation rate of the grain is higher than the slip rate of the grain boundaries. Therefore, the effect of slipping can be ignored. If the strain rate is not sufficient high, the crack of wedge will be released in the triangle grain boundary. So the region of flow instability has insufficient strain rate and high temperature.

At 0.6 strain, there are two regions in the processing maps. The first domain occurs in the region of 350–380 °C for a strain rate 0.003 s^{-1}, with a peak efficiency of about 29 %. The second domain occurs in the region of 380–430 °C for a strain rate range of 0.003 to 0.3 s^{-1}. And the DRX occurs at about 390°C and 0.03 s^{-1}, with a efficiency of about 32 %. The flow instability occurs in the regions of high temperature with a medium strain rate and low temperature with a high strain rate. In these regions, the AZ81E alloy contains the blocking dislocations which are surrounded by particles of rare-earth phase. And the DRX can't eliminate these dislocations completely. With the increase of strain, the density of dislocation is increased and the huge internal stress is developed. When the topical stress exceeds the interfacial bonding strength, the interfacial debonding occurs and the porosity defect shows up. The porosity defect do harm to the mechanical property.

On the basis of hot deformation microstructural studies (Figure 7), it can be concluded that DRX occurs at

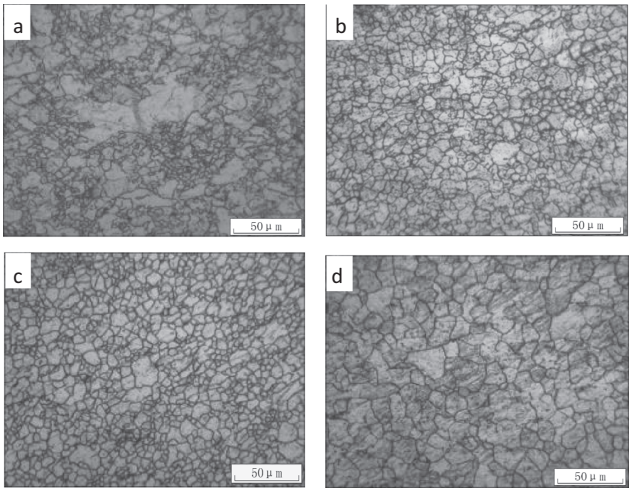

Figure 7: Microstructure characteristics of the hot deformed AZ81E alloys under different conditions: deformed at 400 °C and 0.003 s^{-1} (a), deformed at 400 °C and 0.03 s^{-1} (b), deformed at 400 °C and 0.3 s^{-1} (c), deformed at 430 °C and 0.3 s^{-1} (d).

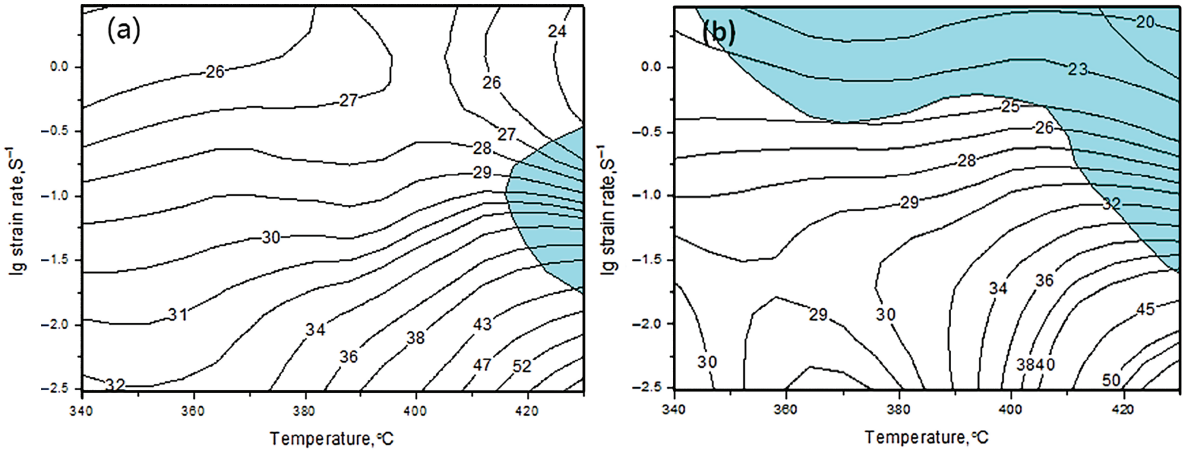

Figure 6: Processing map for different strains for AZ81E alloys: (a) $\varepsilon = 0.4$; (b) $\varepsilon = 0.6$.

the temperature 400 °C and strain rate in the range of 0.03 s^{-1}–0.3 s^{-1}. With the increase of strain rate, the grain size of AZ81E alloys has been decreased. In addition, at temperature 430 °C and strain rate 0.3 s^{-1}, the refining grains become coarse.

According to the power dissipation map and the hot deformation microstructure, the temperature range of 390–400 °C and strain rate range of 0.03–0.3 s^{-1} are the optimum hot working parameters.

Conclusions

(1) The flow stress of AZ81E magnesium alloy decreases with increasing temperature and decreasing strain rate. And the peak stress of AZ81E magnesium alloy moves toward the large strain region with the decline of temperature and the rise of strain rate.

(2) the flow stress equation of AZ81E magnesium alloy is:

$$\sigma = 54.95 \ln \left\{ (Z/8.098\times10^{11})^{1/4.35} + \left[(Z/8.098\times10^{11})^{2/4.35} + 1\right]^{1/2} \right\}$$

where the Z is:

$$Z = \dot{\varepsilon} \exp(166.15\times10^{3})/RT$$

And hot deformation apparent activation energy of the AZ81E alloy is 166.15 kJ/mol, approximately.

(3) At 0.6 strain, the flow instability occurs in the regions of high temperature with a medium strain rate and low temperature with a high strain rate. At 0.4 strain, the flow instability occurs in the regions of high temperature with a medium strain rate.

(4) The flowing deformation instability regions determined by this processing map are as follows: the temperature range of 390–400 °C and strain rate range of 0.03–0.3 s^{-1} are the optimum hot working parameters.

Funding: This paper is supported by Project No. CDJZR14130003 the Fundamental Research Funds for the Central Universities of China.

References

[1] H. Takuda, H. Fujimoto and N. Hatta, J. Mater. Process. Technol., 80 (1998) 513–516.
[2] H. Takuda, T. Enami, K. Kubota and N. Hatta, J. Mater. Process. Technol., 101 (2000) 281–286.
[3] H.M. Liao, S.Y. Long, C.B. Guo and Z.B. Zhu, Trans. Nonferr. Metal. Soc., 18 (2008) S44–S49.
[4] Y.V.R.K. Prasad, H.L. Gegel, S.M. Doraivelu, J.C. Malas, J.T. Morgan, K.A. Lark and D.R. Barker, Metall. Mater. Trans. A., 15 (1984) 1883–1892.
[5] Y.V.R.K. Prasad and T. Seshacharyulu, Int. Mater. Rev., 43 (1998) 243–258.
[6] Y.V.R.K. Prasad, India J. Technol., 28 (1990) 435–451.
[7] S. Mandal, A.K. Bhaduri and V.S. Sarma, Metall. Mater. Trans. A., 43 (2012) 2056–2068.
[8] H. Mirzadeh, J.M. Cabrera and A. Najafizadeh, Acta Mater., 59 (2011) 6441–6448.
[9] D.X. Wen, Y.C. Lin, H.B. Li, X.M. Chen, J. Deng and L.T. Li, Mater. Sci. Eng. A., 591 (2014) 183–192.
[10] Y.Q. Ning, M.W. Fu and X. Chen, Mater. Sci. Eng. A., 540 (2012) 164–173.
[11] D. Samantaray, S. Mandal and A.K. Bhaduri, Mater. Des., 32 (2011) 716–722.
[12] Y.C. Lin, L.T. Li, Y.C. Xia and Y.Q. Jiang, J. Alloys Compd., 550 (2013) 438–445.
[13] C.M. Sellars and W.J.M. Tegart, Mem. Sci. Rev. Metall., 63 (1966) 731–746.
[14] J.K. Chakravartty, G.K. Dey, S. Banerjee and Y.V.R.K. Prasad, J. Nucl. Mater., 218 (1995) 247–255.
[15] M.C. Somani, N.C. Birla, Y.V.R.K. Prasad and V. Singh, J. Mater. Process. Technol., 52 (1995) 225–237.
[16] V.V. Balasubrahmanyam and Y.V.R.K. Prasad, Mater. Sci. Eng. A., 336 (2002) 150–158.